Resonances in e^+e^- annihilation near 2.2 GeV

J. P. Lees,[1] V. Poireau,[1] V. Tisserand,[1] E. Grauges,[2] A. Palano,[3] G. Eigen,[4] D. N. Brown,[5] Yu. G. Kolomensky,[5] M. Fritsch,[6] H. Koch,[6] T. Schroeder,[6] R. Cheaib,[7b] C. Hearty,[7a,7b] T. S. Mattison,[7b] J. A. McKenna,[7b] R. Y. So,[7b] V. E. Blinov,[8a,8b,8c] A. R. Buzykaev,[8a] V. P. Druzhinin,[8a,8b] V. B. Golubev,[8a,8b] E. A. Kozyrev,[8a,8b] E. A. Kravchenko,[8a,8b] A. P. Onuchin,[8a,8b,8c] S. I. Serednyakov,[8a,8b] Yu. I. Skovpen,[8a,8b] E. P. Solodov,[8a,8b] K. Yu. Todyshev,[8a,8b] A. J. Lankford,[9] B. Dey,[10] J. W. Gary,[10] O. Long,[10] A. M. Eisner,[11] W. S. Lockman,[11] W. Panduro Vazquez,[11] D. S. Chao,[12] C. H. Cheng,[12] B. Echenard,[12] K. T. Flood,[12] D. G. Hitlin,[12] J. Kim,[12] Y. Li,[12] T. S. Miyashita,[12] P. Ongmongkolkul,[12] F. C. Porter,[12] M. Röhrken,[12] Z. Huard,[13] B. T. Meadows,[13] B. G. Pushpawela,[13] M. D. Sokoloff,[13] L. Sun,[13,†] J. G. Smith,[14] S. R. Wagner,[14] D. Bernard,[15] M. Verderi,[15] D. Bettoni,[16a] C. Bozzi,[16a] R. Calabrese,[16a,16b] G. Cibinetto,[16a,16b] E. Fioravanti,[16a,16b] I. Garzia,[16a,16b] E. Luppi,[16a,16b] V. Santoro,[16a] A. Calcaterra,[17] R. de Sangro,[17] G. Finocchiaro,[17] S. Martellotti,[17] P. Patteri,[17] I. M. Peruzzi,[17] M. Piccolo,[17] M. Rotondo,[17] A. Zallo,[17] S. Passaggio,[18] C. Patrignani,[18,‡] B. J. Shuve,[19] H. M. Lacker,[20] B. Bhuyan,[21] U. Mallik,[22] C. Chen,[23] J. Cochran,[23] S. Prell,[23] A. V. Gritsan,[24] N. Arnaud,[25] M. Davier,[25] F. Le Diberder,[25] A. M. Lutz,[25] G. Wormser,[25] D. J. Lange,[26] D. M. Wright,[26] J. P. Coleman,[27] E. Gabathuler,[27,*] D. E. Hutchcroft,[27] D. J. Payne,[27] C. Touramanis,[27] A. J. Bevan,[28] F. Di Lodovico,[28] R. Sacco,[28] G. Cowan,[29] Sw. Banerjee,[30] D. N. Brown,[30] C. L. Davis,[30] A. G. Denig,[31] W. Gradl,[31] K. Griessinger,[31] A. Hafner,[31] K. R. Schubert,[31] R. J. Barlow,[32,§] G. D. Lafferty,[32] R. Cenci,[33] A. Jawahery,[33] D. A. Roberts,[33] R. Cowan,[34] S. H. Robertson,[35a,35b] R. M. Seddon,[35b] N. Neri,[36a] F. Palombo,[36a,36b] L. Cremaldi,[37] R. Godang,[37,‖] D. J. Summers,[37] P. Taras,[38] G. De Nardo,[39] C. Sciacca,[39] G. Raven,[40] C. P. Jessop,[41] J. M. LoSecco,[41] K. Honscheid,[42] R. Kass,[42] A. Gaz,[43a] M. Margoni,[43a,43b] M. Posocco,[43a] G. Simi,[43a,43b] F. Simonetto,[43a,43b] R. Stroili,[43a,43b] S. Akar,[44] E. Ben-Haim,[44] M. Bomben,[44] G. R. Bonneaud,[44] G. Calderini,[44] J. Chauveau,[44] G. Marchiori,[44] J. Ocariz,[44] M. Biasini,[45a,45b] E. Manoni,[45a] A. Rossi,[45a] G. Batignani,[46a,46b] S. Bettarini,[46a,46b] M. Carpinelli,[46a,46b,¶] G. Casarosa,[46a,46b] M. Chrzaszcz,[46a] F. Forti,[46a,46b] M. A. Giorgi,[46a,46b] A. Lusiani,[46a,46c] B. Oberhof,[46a,46b] E. Paoloni,[46a,46b] M. Rama,[46a] G. Rizzo,[46a,46b] J. J. Walsh,[46a] L. Zani,[46a,46b] A. J. S. Smith,[47] F. Anulli,[48a] R. Faccini,[48a,48b] F. Ferrarotto,[48a] F. Ferroni,[48a,**] A. Pilloni,[48a,48b] G. Piredda,[48a,*] C. Bünger,[49] S. Dittrich,[49] O. Grünberg,[49] M. Heß,[49] T. Leddig,[49] C. Voß,[49] R. Waldi,[49] T. Adye,[50] F. F. Wilson,[50] S. Emery,[51] G. Vasseur,[51] D. Aston,[52] C. Cartaro,[52] M. R. Convery,[52] J. Dorfan,[52] W. Dunwoodie,[52] M. Ebert,[52] R. C. Field,[52] B. G. Fulsom,[52] M. T. Graham,[52] C. Hast,[52] W. R. Innes,[52,*] P. Kim,[52] D. W. G. S. Leith,[52] S. Luitz,[52] D. B. MacFarlane,[52] D. R. Muller,[52] H. Neal,[52] B. N. Ratcliff,[52] A. Roodman,[52] M. K. Sullivan,[52] J. Va'vra,[52] W. J. Wisniewski,[52] M. V. Purohit,[53] J. R. Wilson,[53] A. Randle-Conde,[54] S. J. Sekula,[54] H. Ahmed,[55] M. Bellis,[56] P. R. Burchat,[56] E. M. T. Puccio,[56] M. S. Alam,[57] J. A. Ernst,[57] R. Gorodeisky,[58] N. Guttman,[58] D. R. Peimer,[58] A. Soffer,[58] S. M. Spanier,[59] J. L. Ritchie,[60] R. F. Schwitters,[60] J. M. Izen,[61] X. C. Lou,[61] F. Bianchi,[62a,62b] F. De Mori,[62a,62b] A. Filippi,[62a] D. Gamba,[62a,62b] L. Lanceri,[63] L. Vitale,[63] F. Martinez-Vidal,[64] A. Oyanguren,[64] J. Albert,[65b] A. Beaulieu,[65b] F. U. Bernlochner,[65b] G. J. King,[65b] R. Kowalewski,[65b] T. Lueck,[65b] I. M. Nugent,[65b] J. M. Roney,[65b] R. J. Sobie,[65a,65b] N. Tasneem,[65b] T. J. Gershon,[66] P. F. Harrison,[66] T. E. Latham,[66] R. Prepost,[67] and S. L. Wu[67]

(*BABAR* Collaboration)

[1]*Laboratoire d'Annecy-le-Vieux de Physique des Particules (LAPP), Université de Savoie, CNRS/IN2P3, F-74941 Annecy-Le-Vieux, France*
[2]*Universitat de Barcelona, Facultat de Fisica, Departament ECM, E-08028 Barcelona, Spain*
[3]*INFN Sezione di Bari and Dipartimento di Fisica, Università di Bari, I-70126 Bari, Italy*
[4]*University of Bergen, Institute of Physics, N-5007 Bergen, Norway*
[5]*Lawrence Berkeley National Laboratory and University of California, Berkeley, California 94720, USA*
[6]*Ruhr Universität Bochum, Institut für Experimentalphysik 1, D-44780 Bochum, Germany*
[7a]*Institute of Particle Physics, Vancouver, British Columbia, Canada V6T 1Z1*
[7b]*University of British Columbia, Vancouver, British Columbia, Canada V6T 1Z1*
[8a]*Budker Institute of Nuclear Physics SB RAS, Novosibirsk 630090, Russia*
[8b]*Novosibirsk State University, Novosibirsk 630090, Russia*
[8c]*Novosibirsk State Technical University, Novosibirsk 630092, Russia*
[9]*University of California at Irvine, Irvine, California 92697, USA*
[10]*University of California at Riverside, Riverside, California 92521, USA*
[11]*University of California at Santa Cruz, Institute for Particle Physics, Santa Cruz, California 95064, USA*
[12]*California Institute of Technology, Pasadena, California 91125, USA*
[13]*University of Cincinnati, Cincinnati, Ohio 45221, USA*
[14]*University of Colorado, Boulder, Colorado 80309, USA*
[15]*Laboratoire Leprince-Ringuet, Ecole Polytechnique, CNRS/IN2P3, F-91128 Palaiseau, France*

[16a]*INFN Sezione di Ferrara, I-44122 Ferrara, Italy*
[16b]*Dipartimento di Fisica e Scienze della Terra, Università di Ferrara, I-44122 Ferrara, Italy*
[17]*INFN Laboratori Nazionali di Frascati, I-00044 Frascati, Italy*
[18]*INFN Sezione di Genova, I-16146 Genova, Italy*
[19]*Harvey Mudd College, Claremont, California 91711, USA*
[20]*Humboldt-Universität zu Berlin, Institut für Physik, D-12489 Berlin, Germany*
[21]*Indian Institute of Technology Guwahati, Guwahati, Assam 781 039, India*
[22]*University of Iowa, Iowa City, Iowa 52242, USA*
[23]*Iowa State University, Ames, Iowa 50011, USA*
[24]*Johns Hopkins University, Baltimore, Maryland 21218, USA*
[25]*Laboratoire de l'Accélérateur Linéaire, IN2P3/CNRS et Université Paris-Sud 11,*
Centre Scientifique d'Orsay, F-91898 Orsay Cedex, France
[26]*Lawrence Livermore National Laboratory, Livermore, California 94550, USA*
[27]*University of Liverpool, Liverpool L69 7ZE, United Kingdom*
[28]*Queen Mary, University of London, London E1 4NS, United Kingdom*
[29]*University of London, Royal Holloway and Bedford New College, Egham, Surrey TW20 0EX,*
United Kingdom
[30]*University of Louisville, Louisville, Kentucky 40292, USA*
[31]*Johannes Gutenberg-Universität Mainz, Institut für Kernphysik, D-55099 Mainz, Germany*
[32]*University of Manchester, Manchester M13 9PL, United Kingdom*
[33]*University of Maryland, College Park, Maryland 20742, USA*
[34]*Massachusetts Institute of Technology, Laboratory for Nuclear Science,*
Cambridge, Massachusetts 02139, USA
[35a]*Institute of Particle Physics, Montréal, Québec, Canada H3A 2T8*
[35b]*McGill University, Montréal, Québec, Canada H3A 2T8*
[36a]*INFN Sezione di Milano, I-20133 Milano, Italy*
[36b]*Dipartimento di Fisica, Università di Milano, I-20133 Milano, Italy*
[37]*University of Mississippi, University, Mississippi 38677, USA*
[38]*Université de Montréal, Physique des Particules, Montréal, Québec, Canada H3C 3J7*
[39]*INFN Sezione di Napoli and Dipartimento di Scienze Fisiche,*
Università di Napoli Federico II, I-80126 Napoli, Italy
[40]*NIKHEF, National Institute for Nuclear Physics and High Energy Physics, NL-1009 DB Amsterdam,*
The Netherlands
[41]*University of Notre Dame, Notre Dame, Indiana 46556, USA*
[42]*Ohio State University, Columbus, Ohio 43210, USA*
[43a]*INFN Sezione di Padova, I-35131 Padova, Italy*
[43a]*Dipartimento di Fisica, Università di Padova, I-35131 Padova, Italy*
[44]*Laboratoire de Physique Nucléaire et de Hautes Energies, Sorbonne Université,*
Paris Diderot Sorbonne Paris Cité, CNRS/IN2P3, F-75252 Paris, France
[45a]*INFN Sezione di Perugia, I-06123 Perugia, Italy*
[45b]*Dipartimento di Fisica, Università di Perugia, I-06123 Perugia, Italy*
[46a]*INFN Sezione di Pisa, I-56127 Pisa, Italy*
[46b]*Dipartimento di Fisica, Università di Pisa, I-56127 Pisa, Italy*
[46c]*Scuola Normale Superiore di Pisa, I-56127 Pisa, Italy*
[47]*Princeton University, Princeton, New Jersey 08544, USA*
[48a]*INFN Sezione di Roma, I-00185 Roma, Italy*
[48b]*Dipartimento di Fisica, Università di Roma La Sapienza, I-00185 Roma, Italy*
[49]*Universität Rostock, D-18051 Rostock, Germany*
[50]*Rutherford Appleton Laboratory, Chilton, Didcot, Oxon, OX11 0QX, United Kingdom*
[51]*IRFU, CEA, Université Paris-Saclay, F-91191 Gif-sur-Yvette, France*
[52]*SLAC National Accelerator Laboratory, Stanford, California 94309 USA*
[53]*University of South Carolina, Columbia, South Carolina 29208, USA*
[54]*Southern Methodist University, Dallas, Texas 75275, USA*
[55]*St. Francis Xavier University, Antigonish, Nova Scotia, Canada B2G 2W5*
[56]*Stanford University, Stanford, California 94305, USA*
[57]*State University of New York, Albany, New York 12222, USA*
[58]*Tel Aviv University, School of Physics and Astronomy, Tel Aviv, 69978, Israel*
[59]*University of Tennessee, Knoxville, Tennessee 37996, USA*
[60]*University of Texas at Austin, Austin, Texas 78712, USA*
[61]*University of Texas at Dallas, Richardson, Texas 75083, USA*

[62a]INFN Sezione di Torino, I-10125 Torino, Italy

[62b]Dipartimento di Fisica, Università di Torino, I-10125 Torino, Italy

[63]INFN Sezione di Trieste and Dipartimento di Fisica, Università di Trieste, I-34127 Trieste, Italy

[64]IFIC, Universitat de Valencia-CSIC, E-46071 Valencia, Spain

[65a]Institute of Particle Physics, Victoria, British Columbia, Canada V8W 3P6

[65b]University of Victoria, Victoria, British Columbia, Canada V8W 3P6

[66]Department of Physics, University of Warwick, Coventry CV4 7AL, United Kingdom

[67]University of Wisconsin, Madison, Wisconsin 53706, USA

Using the initial-state radiation method, the $e^+e^- \to K_S K_L$ cross section from 1.98 to 2.54 GeV is measured in a data sample of 469 fb^{-1} collected with the *BABAR* detector. The results are used in conjunction with previous *BABAR* results for the $e^+e^- \to K^+K^-$, $e^+e^- \to \pi^+\pi^-$, $e^+e^- \to \pi^+\pi^-\eta$, and $e^+e^- \to \omega\pi\pi$ cross sections to investigate the nature of the resonance structure recently observed by the BESIII experiment in the $e^+e^- \to K^+K^-$ cross section.

I. INTRODUCTION

Recently, a precise measurement of the $e^+e^- \to K^+K^-$ cross section in the center-of-mass (c.m.) energy range $E = 2.00\text{--}3.08$ GeV was performed by the BESIII Collaboration [1]. In this cross section, a clear interference pattern was observed near 2.2 GeV. To explain this pattern, BESIII inferred the existence of a resonance with a mass of $2239 \pm 7 \pm 11 \text{ MeV}/c^2$ and a width of $140 \pm 12 \pm 21$ MeV. In the Particle Data Group (PDG) table [2] there are two vector resonances with a mass near 2.2 GeV/c^2: $\phi(2170)$ and $\rho(2150)$. The first is observed in three reactions: $e^+e^- \to \phi(2170)$ [3,4], $J/\psi \to \eta\phi(2170)$ [5,6], and $e^+e^- \to \eta\phi(2170)$ [7], but only in the decay mode $\phi(2170) \to \phi(1020)f_0(980)$. As shown in Ref. [1], the parameters of the resonance structure observed in the $e^+e^- \to K^+K^-$ cross section differ from the $\phi(2170)$ PDG parameters by more than 3σ in mass and more than 2σ in width. The isovector resonance $\rho(2150)$ is not well established. The PDG lists three e^+e^- annihilation processes in which evidence for its existence is seen: $e^+e^- \to f_1(1275)\pi^+\pi^-$, $e^+e^- \to \eta'\pi^+\pi^-$, and $e^+e^- \to \pi^+\pi^-$. In the first two

reactions, wide ($\Gamma \sim 300$ MeV) resonancelike structures are observed near the reaction thresholds [8]. A completely different structure is seen in the third process. A resonance with mass and width 2254 ± 22 MeV/c^2 and 109 ± 76 MeV, respectively, is needed to describe the interference pattern in the $e^+e^- \to \pi^+\pi^-$ cross section [9]. Note that the parameters of this resonance are very similar to those mentioned above for the $e^+e^- \to K^+K^-$ reaction from BESIII.

Any resonance in the $e^+e^- \to K^+K^-$ cross section should also be present in $e^+e^- \to K_S K_L$. The most precise data on this reaction near 2 GeV were obtained by the *BABAR* Collaboration [10]. In this previous work, the $e^+e^- \to K_S K_L$ cross section was measured up to 2.2 GeV. Above 2 GeV, the cross section was found to be consistent with zero within the statistical uncertainties of around 20 pb. In the present work we expand the energy region of the *BABAR* $K_S K_L$ measurement up to 2.5 GeV. The new $K_S K_L$ measurements, in conjunction with previous *BABAR* results for other exclusive e^+e^- processes, are used to investigate the nature of the structure observed by BESIII in $e^+e^- \to K^+K^-$.

II. FIT TO THE BESIII AND *BABAR* $e^+e^- \to K^+K^-$ DATA

In Fig. 1 we show BESIII [1] and *BABAR* [11] data on the dressed Born cross section for the process $e^+e^- \to K^+K^-$ in the energy region of interest. The dressed cross section used to obtain resonance parameters is calculated from the bare cross section (σ_b) listed in Refs. [1,11] as $\sigma = \sigma_b R_{VP}/C_{FS}$, where R_{VP} is the factor taking into account the vacuum polarization correction, while C_{FS} is the final-state correction (see, e.g., Ref. [12]). The latter, in particular, takes into account extra photon radiation from the final state. In the energy region of interest, 2.00– 2.5 GeV, $R_{VP} \approx 1.04$ and $C_{FS} = 1.008$. The BESIII and
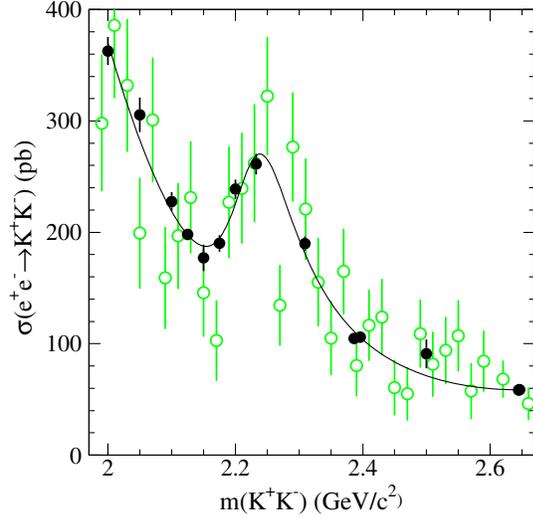

FIG. 1. The $e^+e^- \to K^+K^-$ cross section measured by BESIII [1] (filled circles) and *BABAR* [11] (open circles). The curve is the result of the fit to a coherent sum of resonant and nonresonant contributions (see text).

BABAR data on the dressed $e^+e^- \to K^+K^-$ cross section are fitted by a coherent sum of resonant and nonresonant contributions

$$\sigma(E) = \frac{M_R^2 \beta(E)^3}{E^2 \beta(M_R)^3} |\sqrt{\sigma_R} BW(E) + e^{i\varphi} P(E)|^2, \quad (1)$$

where $\beta(E) = \sqrt{1 - 4m_K^2/E^2}$, m_K is the charged kaon mass, $BW(E) = M_R \Gamma_R / (M_R^2 - E^2 - iE\Gamma_R)$ is the Breit-Wigner function describing the resonant amplitude, M_R, Γ_R, and σ_R are the resonance mass, width, and peak cross section, $P(E)$ is a second-order polynomial describing the nonresonant amplitude, and φ is the relative phase between the resonant and nonresonant amplitudes. The fit result is shown in Fig. 1. The fit yields $\chi^2/\nu = 55.8/40$ ($P(\chi^2) = 5\%$) and the fit parameters are listed in Table I.

The systematic uncertainties in the resonance parameters come mainly from uncertainties in the description of the resonance and nonresonance shapes. The uncertainty due to the absolute c.m. energy calibration is negligible [1,11]. For the signal shape we study the effect of the energy-dependent width assuming that the main resonance decay mode is either K^+K^- or $\eta\rho$. We also use another parametrization of the nonresonance amplitude, in which the

TABLE I. The parameters for the fit to the $e^+e^- \to K^+K^-$ cross section data from BESIII and *BABAR*. The quoted uncertainties are statistical and systematic, respectively.

M_R	$2227 \pm 9 \pm 9$ MeV/c^2
Γ_R	$127 \pm 14 \pm 4$ MeV
σ_R	$39 \pm 6 \pm 4$ pb
φ	$143 \pm 8 \pm 9$ deg

main energy dependence is given by the function $a/(E^2 - b^2)$ inspired by the vector-meson dominance model, where a and b are fitted parameters, while small deviations from the main dependence are described by a quadratic polynomial. The nonresonance amplitude may have an energy-dependent imaginary part originating from vector resonances lying below 2 GeV. Using the results of Ref. [13], we estimate that its fraction reaches 10% at 2 GeV and decreases to 5% at 2.5 GeV. To study the effect of the imaginary parts, we multiply the function $P(E)$ in Eq. (1) by a factor of $1 \pm iG(E)$, where $G(E)$ is a linear function decreasing from 0.05–0.15 at $E = 2$ GeV to zero at 2.5 GeV. The deviations from the nominal parameter values listed in Table I are taken as the estimates of the systematic uncertainties given in Table I. The systematic uncertainty in the parameter σ_R includes also the correlated systematic uncertainty in the $e^+e^- \to K^+K^-$ cross section, which is 2.5% (6%) for the BESIII (*BABAR*) data.

Our values for the resonance mass and width are close to the values $2239 \pm 7 \pm 11$ MeV/c^2 and $140 \pm 12 \pm 21$ MeV obtained in Ref. [1]. We also perform the fit to the *BABAR* data only. The resulting parameters are $M_R = 2201 \pm 19$ MeV/c^2, $\Gamma_R = 70 \pm 38$ MeV, and $\sigma_R = 42^{+29}_{-16}$ pb. The resonance significance in the *BABAR* data estimated from the χ^2 difference for the fits with and without the resonance contribution is 3.5σ.

III. THE $e^+e^- \to K_S K_L$ CROSS SECTION IN THE 2.0–2.5 GeV ENERGY RANGE

The data analysis presented in this paper is based on methods developed for the measurement of the $e^+e^- \to K_S K_L$ cross section in Ref. [10]. The data set, with an integrated luminosity of 469 fb^{-1} [14], was collected with the *BABAR* detector [15] at the SLAC PEP-II asymmetric-energy e^+e^- storage ring at the $\Upsilon(4S)$ resonance and 40 MeV below this resonance. The initial-state-radiation (ISR) technique is used, in which the cross section for the process $e^+e^- \to K_S K_L$ is determined from the $K_S K_L$ invariant mass spectrum measured in the reaction $e^+e^- \to K_S K_L \gamma$.

The selection criteria for $e^+e^- \to K_S K_L \gamma$ events are described in detail in Ref. [10]. We require the detection of all the final-state particles. The ISR photon candidate must have an energy in the c.m. frame greater than 3 GeV. The K_S candidate is reconstructed using the $K_S \to \pi^+\pi^-$ decay mode. Two oppositely charged tracks not identified as electrons are fitted to a common vertex. The distance between the reconstructed K_S decay vertex and the beam axis must be in the range from 0.2 to 40.0 cm. The cosine of the angle between a vector from the beam interaction point to the K_S vertex and the K_S momentum in the plane transverse to the beam axis is required to be larger than 0.9992. The invariant mass of the K_S candidate must be in the range 0.482–0.512 GeV/c^2. The K_L candidate is a
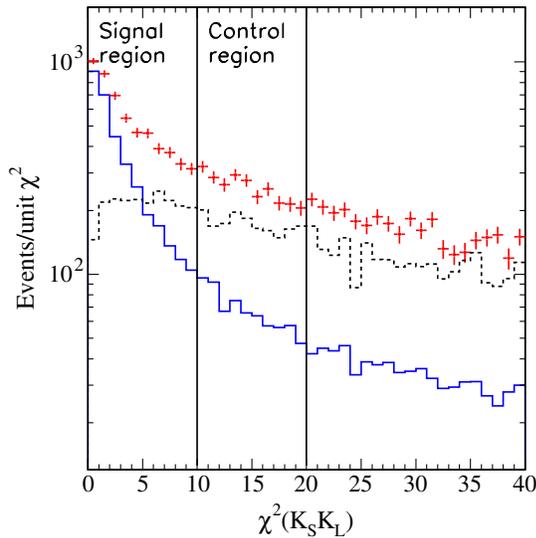
FIG. 2. The kinematic-fit χ^2 distribution for selected data events with $1.06 < m(K_S K_L) < 2.5$ GeV/c^2 (points with error bars). The hatched histogram represents the simulated background contribution. The solid histogram shows the simulated signal distribution. The vertical lines indicate the boundaries of the signal and control regions.

cluster in the calorimeter with energy deposition greater than 0.2 GeV. To suppress background, we also require the event to not contain extra charged tracks originating from the interaction region or extra photons with energy larger than 0.5 GeV.

The ISR photon, K_S, and K_L candidates are subjected to a three-constraint kinematic fit to the $e^+e^- \to K_S K_L \gamma$ hypothesis with the requirement of energy and momentum balance. Only the angular information is used in the fit for the K_L candidate. If there are several K_L candidates in an event, the $K_S K_L \gamma$ combination giving the smallest χ^2 value is retained. The particle parameters after the kinematic fit are used to calculate the $K_S K_L$ invariant mass $m(K_S K_L)$, which is required to satisfy $1.06 < m(K_S K_L) < 2.5$ GeV/c^2.

The χ^2 distribution from the fit for the selected events is shown in Fig. 2 in comparison with the simulated signal and background distributions. The background is dominated by the ISR processes $e^+e^- \to K_S K_L \pi^0 \gamma$, $K_S K_L \eta \gamma$, and $K_S K_L \pi^0 \pi^0 \gamma$. The condition $\chi^2 < 10$ is applied to select signal events. The control region $10 < \chi^2 < 20$ is used to estimate and subtract background. The numbers of signal (N_s) and background (N_b) events in the signal region ($\chi^2 < 10$) are determined as

$$N_s = N_1 - N_b, N_b = (N_2 - aN_s)/b, \qquad (2)$$

where N_1 and N_2 are the numbers of selected data events in the signal and control regions, and $a = 0.20 \pm 0.01$ and $b = 0.87 \pm 0.09$ are the N_2/N_1 ratios for signal and background, respectively.

The value of the coefficient a is determined from the simulated signal χ^2 distribution. For the mass region of

interest $2.0 < m(K_S K_L) < 2.5$ GeV/c^2, where the number of signal events is small, the aN_s term in the expression for N_b is negligible. The coefficient b is determined in two ways: either using background simulation, or from the difference between the data and simulated signal distributions in Fig. 2. The signal distribution is normalized to the number of data events with $\chi^2 < 3$ after subtraction of the background estimated from simulation. The average of the two b values is quoted above. Their difference (10%) is taken as an estimate of the systematic uncertainty in b. As shown in Ref. [10], the background $m(K_S K_L)$ distribution obtained using Eq. (2) is found to be in reasonable agreement with the same distribution obtained from simulation.

The background estimated from the control region decreases monotonically with increasing $m(K_S K_L)$ and is well approximated by a smooth function. Figure 3 shows the $m(K_S K_L)$ distribution for data events from the signal region. The curve represents the estimated background distribution.

The uncertainty in the background is 12%, which includes the 10% uncertainty in the parameter b in Eq. (2) and a 6% uncertainty in the background approximation. We do not see a significant signal of $K_S K_L$ events over background. The $e^+e^- \to K_S K_L$ cross section in the mass region $1.96 < m(K_S K_L) < 2.56$ GeV/c^2 obtained from the mass spectrum in Fig. 3 after background subtraction is shown in Fig. 4 (left). The details on the detection efficiency and ISR luminosity can be found in Ref. [10]. The numerical values of the $e^+e^- \to K_S K_L$ cross section, with statistical and systematic uncertainties, are listed in Table II. The systematic uncertainties arise mainly from the background subtraction and are fully correlated between different $m(K_S K_L)$ intervals.
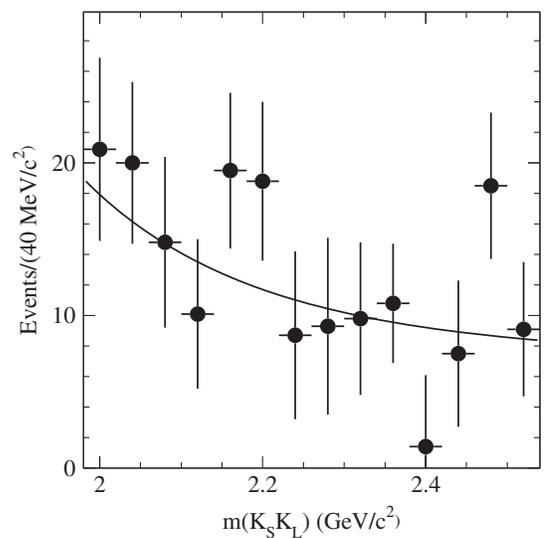

FIG. 3. The $m(K_S K_L)$ distribution for data events with $\chi^2 < 10$. The curve represents background estimated from the control region.
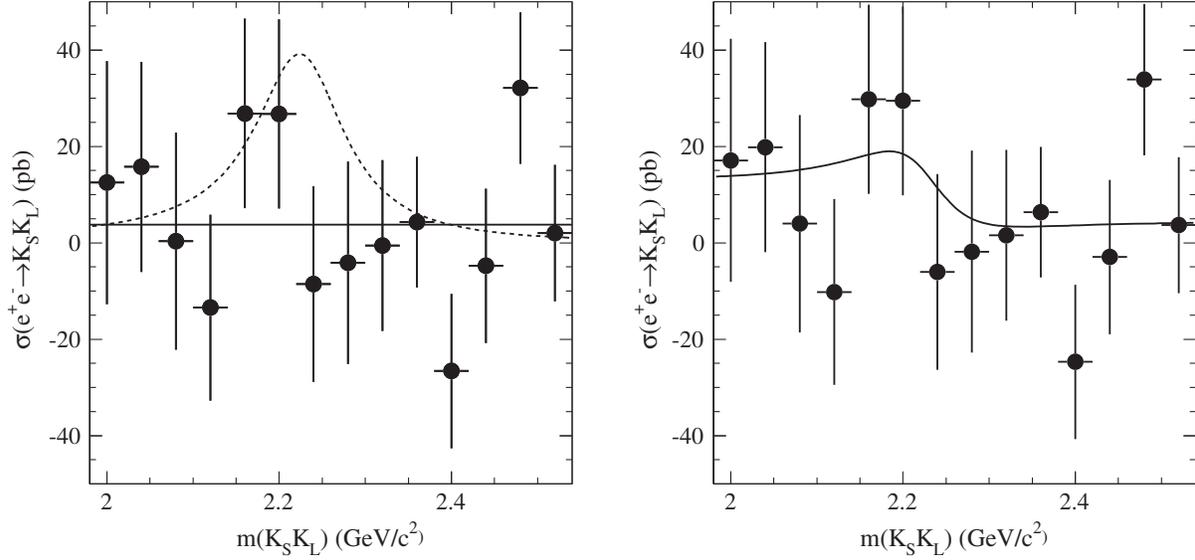
FIG. 4. Left panel: The measured $e^+e^- \to K_S K_L$ cross section fitted with a constant (solid line). The dashed curve represents the resonance line shape with the parameters listed in Table I. Right panel: The curve is the result of the fit to the $e^+e^- \to K_S K_L$ data with a coherent sum of a resonant amplitude with the parameters listed in Table I and a nonresonant constant amplitude. The points with error bars represent the data following subtraction of the background, which has been scaled by a factor of 0.94 (see text).

A fit to the cross section data with a constant yields $\chi^2/\nu = 11.7/13$, where ν is the number of degrees of freedom. The average value of the $e^+e^- \to K_S K_L$ cross section between 1.98 and 2.54 GeV/c^2 is found to be $(4 \pm 5 \pm 5)$ pb, which is therefore consistent with zero. The dashed curve in Fig. 4 (left) represents the cross section for the resonance with the parameters listed in Table I. Formally, from the χ^2 difference between the two hypotheses in Fig. 4 (left) the resonance interpretation can be excluded at 2.3σ. However, possible destructive interference between the resonant and nonresonant $e^+e^- \to K_S K_L$ amplitudes may significantly weaken this constraint. We also must take into account the uncertainty in the background subtraction and the statistical uncertainty in the resonance cross section obtained from the fit to the $e^+e^- \to K^+K^-$ data. To do this we fit the mass spectrum shown in Fig. 3 with a sum of signal and background distributions. The background distribution shown in Fig. 3 is multiplied by a scale factor r_{bkg}, which is allowed to vary within a 12%

uncertainty around unity. The signal cross section is described by Eq. (1) with a constant nonresonant amplitude $P(E) = \sqrt{\sigma_{NR}}$ and the parameter σ_R varied around the value listed in Table I. From the fit we determine σ_{NR} and φ. The result of the fit is shown by the curve in Fig. 4 (right). The fitted value of the parameter r_{bkg} is 0.94. Therefore, the points in Fig. 4 (right) lie slightly higher than those in Fig. 4 (left). The fit yields $\chi^2/\nu = 11.0/12$ and the following values of parameters:

$$\sigma_{NR} = 7.3^{+7.4}_{-5.3} \text{ pb}, \qquad \varphi = (-69 \pm 23)°. \qquad (3)$$

We conclude that the *BABAR* data on the $e^+e^- \to K_S K_L$ cross section do not exclude the existence of the resonance with the parameters listed in Table I, but restrict the possible range of allowed values of the relative phase between the resonant and nonresonant $e^+e^- \to K_S K_L$ amplitudes.

TABLE II. The $m(K_S K_L)$ interval and measured Born cross sections for the processes $e^+e^- \to K_S K_L$. The quoted uncertainties are statistical and systematic, respectively.

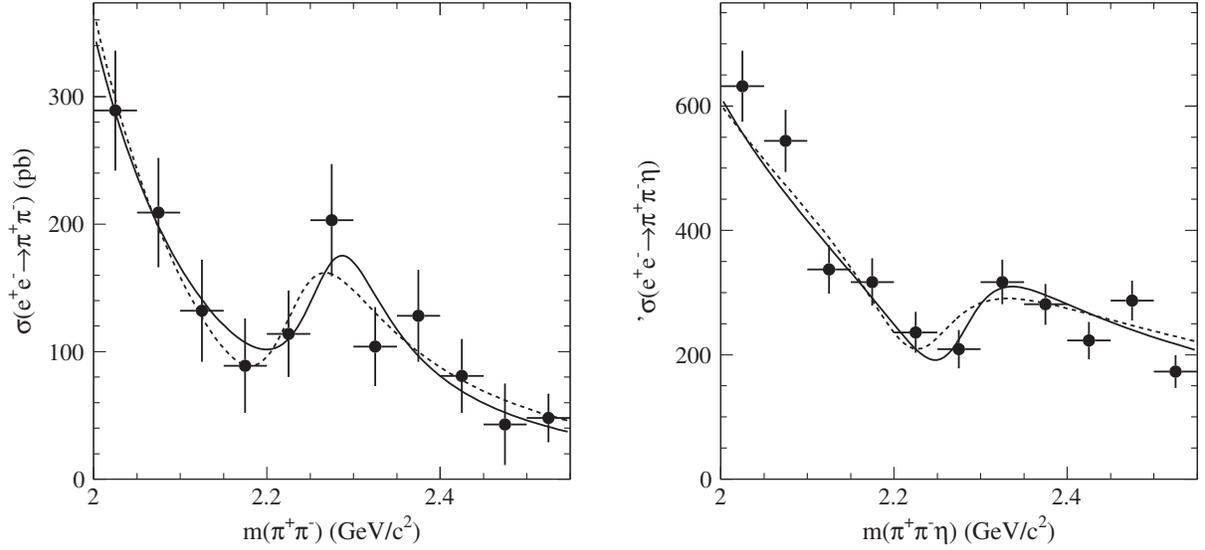| $m(K_S K_L)$ (GeV/c^2)	σ (pb)	$m(K_S K_L)$ (GeV/c^2)	σ (pb)
1.98–2.02	$12.5 \pm 25.2 \pm 9.2$	2.26–2.30	$-4.1 \pm 21.0 \pm 4.6$
2.02–2.06	$15.8 \pm 21.8 \pm 8.1$	2.30–2.34	$-0.6 \pm 17.7 \pm 4.3$
2.06–2.10	$0.4 \pm 22.5 \pm 7.2$	2.34–2.38	$4.3 \pm 13.5 \pm 4.0$
2.10–2.14	$-13.4 \pm 19.3 \pm 6.5$	2.28–2.42	$-26.6 \pm 16.0 \pm 3.8$
2.14–2.18	$26.9 \pm 19.6 \pm 5.9$	2.42–2.46	$-4.8 \pm 16.0 \pm 3.6$
2.18–2.22	$26.8 \pm 19.6 \pm 5.4$	2.46–2.50	$32.1 \pm 15.7 \pm 3.5$
2.22–2.26	$-8.6 \pm 20.3 \pm 5.0$	2.50–2.54	$2.0 \pm 14.1 \pm 3.3$

FIG. 5. Left panel: The $e^+e^- \to \pi^+\pi^-$ cross section measured by *BABAR* [9]. Right panel: The $e^+e^- \to \pi^+\pi^-\eta$ cross section measured by *BABAR* [16]. The solid curves are the results of the simultaneous fit to the $e^+e^- \to \pi^+\pi^-$ and $\pi^+\pi^-\eta$ cross section data, while the dashed curves represent the results of the simultaneous fit to the $e^+e^- \to K^+K^-$, $\pi^+\pi^-$, and $\pi^+\pi^-\eta$ cross section data.

IV. SIMULTANEOUS FIT TO THE $e^+e^- \to K^+K^-$, $\pi^+\pi^-$, AND $\pi^+\pi^-\eta$ DATA WITH AN ISOVECTOR RESONANCE

As discussed in the Introduction, the mass and width of the resonance observed in the process $e^+e^- \to K^+K^-$ near 2.2 GeV are close to the parameters of the state seen in the $e^+e^- \to \pi^+\pi^-$ cross section measured by *BABAR* [9]. The latter cross section in the energy range 2.00–2.55 GeV is shown in Fig. 5 (left). An interference pattern in the energy region near 2.25 GeV is also seen in the energy dependence of the $e^+e^- \to \pi^+\pi^-\eta$ cross section recently measured by *BABAR* [16] and shown in Fig. 5 (right). We perform a simultaneous fit to the $e^+e^- \to \pi^+\pi^-$ and $\pi^+\pi^-\eta$ data. The cross sections are described by formulas similar to Eq. (1). For the $\pi^+\pi^-\eta$ channel, the phase space factor $\beta(E)^3/\beta(M_R)^3$ in Eq. (1) is replaced by the factor $p_\eta(E)^3/p_\eta(M_R)^3 M_R/E$ [17], where p_η is the η-meson momentum

calculated in the model of the $\rho(770)\eta$ intermediate state. The nonresonant amplitude is described by the function $a/(E^2 - b^2)$ inspired by the vector-meson dominance model. The ten fitted parameters are the mass (M_R) and width (Γ_R) of the resonance, the peak cross sections [$\sigma(e^+e^- \to R \to \pi^+\pi^-)$ and $\sigma(e^+e^- \to R \to \pi^+\pi^-\eta)$], and a, b, and φ for the two channels. The result of the fit is shown in Fig. 5 by the solid curves. The fit parameters obtained are listed in the second column of Table III. The fit yields $\chi^2/\nu = 14.0/12$ ($P(\chi^2) = 0.30$). The significance of the resonance calculated from the difference in χ^2 with and without the resonance contributions is 4.6σ. The systematic uncertainties in the resonance parameters are determined as described in Sec. II.

We also perform a simultaneous fit to the BESIII and *BABAR* $e^+e^- \to K^+K^-$ data and the *BABAR* $e^+e^- \to \pi^+\pi^-$ and $\pi^+\pi^-\eta$ data. The $e^+e^- \to K^+K^-$ cross

TABLE III. The parameters for the fit to the $e^+e^- \to \pi^+\pi^-$ and $\pi^+\pi^-\eta$ cross section data (second column), and to the $e^+e^- \to K^+K^-$, $\pi^+\pi^-$, and $\pi^+\pi^-\eta$ cross section data (third column). The quoted uncertainties are statistical and systematic, respectively.

	$\pi^+\pi^-$ and $\pi^+\pi^-\eta$	K^+K^-, $\pi^+\pi^-$, and $\pi^+\pi^-\eta$
M_R (MeV/c^2)	$2270 \pm 20 \pm 9$	$2232 \pm 8 \pm 9$
Γ_R (MeV)	$116^{+90}_{-60} \pm 50$	$133 \pm 14 \pm 4$
$\sigma(e^+e^- \to R \to K^+K^-)$ (pb)	$\cdots$	$41 \pm 6 \pm 4$
$\sigma(e^+e^- \to R \to \pi^+\pi^-)$ (pb)	$34^{+26}_{-19} \pm 4$	$36^{+27}_{-20} \pm 4$
$\sigma(e^+e^- \to R \to \pi^+\pi^-\eta)$ (pb)	$33^{+34}_{-13} \pm 4$	$27^{+14}_{-11} \pm 4$
$\varphi(e^+e^- \to K^+K^-)$ (deg)	$\cdots$	$140 \pm 8 \pm 9$
$\varphi(e^+e^- \to \pi^+\pi^-)$ (deg)	$147 \pm 30 \pm 10$	$188 \pm 19 \pm 9$
$\varphi(e^+e^- \to \pi^+\pi^-\eta)$ (deg)	$217 \pm 24 \pm 9$	$251 \pm 15 \pm 9$
χ^2/ν	$13.96/12$	$17.2/14$

section is parametrized as described in Sec. II. The fit parameters obtained are listed in the third column of Table III. Since the $e^+e^- \to K^+K^-$ data are statistically more accurate than the $\pi^+\pi^-$ or $\pi^+\pi^-\eta$ data, the fitted resonance mass, width, and $\sigma(e^+e^- \to R \to K^+K^-)$ are similar to those (Table I) obtained in the fit to the K^+K^- data alone. The results of the fit for $e^+e^- \to \pi^+\pi^-$ and $\pi^+\pi^-\eta$ cross sections are shown in Fig. 5 by the dashed curves. The χ^2/ν calculated using the $\pi^+\pi^-$ and $\pi^+\pi^-\eta$ data is 17.2/14 $(P(\chi^2) = 0.25)$. We conclude that it is very likely that the interference patterns observed in the three cross sections discussed above are manifestations of the same isovector resonance, $\rho(2230)$. It is interesting to note that the decay rates of this state to K^+K^-, $\pi^+\pi^-$, and $\pi^+\pi^-\eta$ are all similar.

V. TWO-RESONANCE FIT

The isovector state discussed in the previous section is expected to have an ω-like isoscalar partner with a similar mass. An indication of an isoscalar resonance structure near 2.25 GeV is seen in the $e^+e^- \to \omega\pi^+\pi^-$ and $e^+e^- \to \omega\pi^0\pi^0$ cross sections measured by *BABAR* [8,18]. The energy dependence of the total $e^+e^- \to \omega\pi\pi$ ($\omega\pi^+\pi^-+\omega\pi^0\pi^0$) cross section in the energy region of interest is shown in Fig. 6. It is fitted by a coherent sum of resonant and nonresonant contributions. We assume that the process $e^+e^- \to \omega\pi\pi$ proceeds via the $\omega f_0(500)$ intermediate state. Therefore, the factor $\beta(E)^3/\beta(M_R)^3$ in Eq. (1) is replaced by the s-wave phase-space factor $p_\omega(E)/p_\omega(M_R)$, where p_ω is the ω-meson momentum in $e^+e^- \to \omega f_0(500)$. It should be noted that the phase-space factor for the other possible intermediate state, $b_1(1235)\pi$, has a similar energy dependence in the energy region of interest. The nonresonant amplitude is described by the function $a/(E^2 - b^2)$. The fit yields $\chi^2/\nu = 6.8/6$. The result of the fit is shown in Fig. 6 by the solid curve. The fitted resonance mass $(2265 \pm 20$ MeV/$c^2)$ and width $(75^{+125}_{-27}$ MeV) are similar to the parameters of the isovector state in Table III. Since different intermediate mechanisms (e.g., ωf_0 and $b_1\pi$) contribute to the $\omega\pi\pi$ final state, the resonant and nonresonant amplitudes may be not fully coherent. Inclusion in the fit of an incoherent contribution describing up to 50% of the nonresonant cross section has an insignificant impact on the fitted resonance mass and width. The dashed curve in Fig. 6 is the result of the fit to data with a second-order polynomial. The χ^2/ν for this fit is 18.1/9. From the χ^2 difference between the two fits we estimate that the significance of the resonance signal in the $e^+e^- \to \omega\pi\pi$ cross section is 2.6σ.

From isospin invariance, the isovector amplitude enters the $e^+e^- \to K^+K^-$ and $e^+e^- \to K_S K_L$ amplitudes with the opposite sign (in contrast to the isoscalar case) [19]:
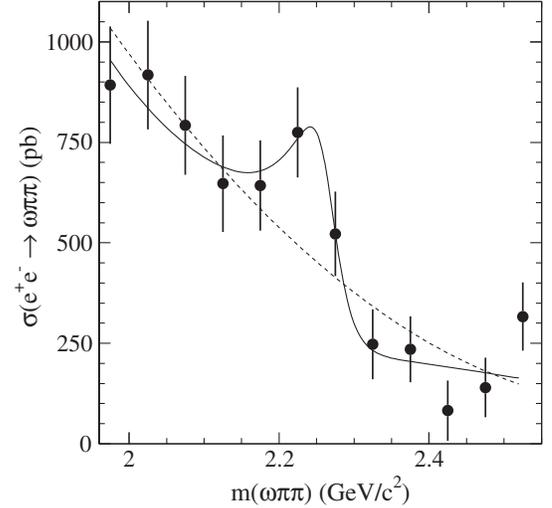

FIG. 6. The $e^+e^- \to \omega\pi\pi$ cross section measured by *BABAR* [8,18]. The solid curve is the result of the fit by a coherent sum of resonant and nonresonant contributions, while the dashed curve represents the results of the fit to a quadratic polynomial.

$$A(e^+e^- \to K^+K^-) = A_{I=0} + A_{I=1},$$
$$A(e^+e^- \to K_S K_L) = A_{I=0} - A_{I=1}. \tag{4}$$

The quark model predicts [19] that the isoscalar amplitude related to the ω-like resonance is one-third the amplitude of the corresponding ρ-like state and that these amplitudes have the same sign in the $e^+e^- \to K^+K^-$ channel. If the ρ- and ω-like resonances have similar masses and widths, we expect the resonance amplitude in the $e^+e^- \to K_S K_L$ reaction to be about two times smaller than that in $e^+e^- \to K^+K^-$. This weakens the constraints on the nonresonant $e^+e^- \to K_S K_L$ cross sections and the interference phase, relation (3), obtained in the fit to the $e^+e^- \to K_S K_L$ data in Sec. [10]. Repeating this fit with the resonance amplitude smaller by a factor of two, we obtain $\chi^2/\nu = 10.6/12$ and the parameters

$$\sigma_{\mathrm{NR}} = 5.0^{+8.2}_{-4.8}, \qquad \varphi = (-51^{+56}_{-41})^\circ. \tag{5}$$

The fit with the zero nonresonant cross section also has an acceptable χ^2 value, 12.1/14. We conclude that the two-resonance fit allows a simultaneous description of the $e^+e^- \to K^+K^-$ and $e^+e^- \to K_S K_L$ data without strong constraints on the interference parameters in the $e^+e^- \to K_S K_L$ channel.

Finally, we fit the $e^+e^- \to K^+K^-$, $e^+e^- \to \pi^+\pi^-$, and $e^+e^- \to \pi^+\pi^-\eta$ data using the model described in Sec. IV with an additional contribution from the $\phi(2170)$ resonance. The $\phi(2170)$ mass and width are fixed at their PDG values [2]. The inclusion of the $\phi(2170)$ has an insignificant impact on the quality of the fit. The fitted value of the $\phi(2170)$ peak cross section is found to be consistent with zero, $0.8^{+2.9}_{-0.8}$ pb.

VI. SUMMARY

In this paper, we present measurements of the $e^+e^- \to K_S K_L$ cross section in the center-of-mass range from 1.98 to 2.54 GeV. The measured cross section is consistent with zero and does not exhibit evidence for a resonance structure. The $K_S K_L$ data are analyzed in conjunction with BESIII [1] and *BABAR* [11] data on the $e^+e^- \to K^+K^-$ cross section, and with *BABAR* data on the $e^+e^- \to \pi^+\pi^-$ [9], $\pi^+\pi^-\eta$ [16], $\omega\pi^+\pi^- + \omega\pi^0\pi^0$ [8,18] cross sections to examine properties and better elucidate the nature of the resonance structure observed by BESIII in the $e^+e^- \to K^+K^-$ cross section near 2.25 GeV [1].

The interference patterns seen in the $e^+e^- \to \pi^+\pi^-$ and $e^+e^- \to \pi^+\pi^-\eta$ data near 2.25 GeV provide 4.6σ evidence for the existence of the isovector resonance $\rho(2230)$. Its mass and width are consistent with the parameters of the resonance observed in the $e^+e^- \to K^+K^-$ channel. All three cross sections are well described by a model with $\rho(2230)$ mass and width $M = 2232 \pm 8 \pm 9$ MeV/c^2 and $\Gamma = 133 \pm 14 \pm 4$ MeV.

Any resonance in the $e^+e^- \to K^+K^-$ cross section should also be manifest in the $e^+e^- \to K_S K_L$ cross section. The *BABAR* data on the $e^+e^- \to K_S K_L$ cross section do not exclude the existence of the $\rho(2230)$ resonance, but strongly restrict the possible range of allowed values of the relative phase between the resonant and nonresonant $e^+e^- \to K_S K_L$ amplitudes. This restriction may be significantly weakened by inclusion in the fit of an additional isoscalar resonance with a nearby mass. An indication of such a resonance with 2.6σ significance is seen in the $e^+e^- \to \omega\pi\pi$ cross section.

Further study of the resonance structures near 2.25 GeV can be performed at the BESIII experiment, where the cross sections for $e^+e^- \to \pi^+\pi^-\eta$, $\omega\pi^+\pi^-$, $\omega\pi^0\pi^0$ and other exclusive processes in the energy range between 2 and 2.5 GeV may be measured with high accuracy.

[1] M. Ablikim *et al.* (BESIII Collaboration), Phys. Rev. D **99**, 032001 (2019).

[2] M. Tanabashi *et al.* (Particle Data Group), Phys. Rev. D **98**, 030001 (2018).

[3] J. P. Lees *et al.* (*BABAR* Collaboration), Phys. Rev. D **86**, 012008 (2012).

[4] C. P. Shen *et al.* (Belle Collaboration), Phys. Rev. D **80**, 031101 (2009).

[5] M. Ablikim *et al.* (BES Collaboration), Phys. Rev. Lett. **100**, 102003 (2008).

[6] M. Ablikim *et al.* (BESIII Collaboration), Phys. Rev. D **91**, 052017 (2015).

[7] M. Ablikim *et al.* (BESIII Collaboration), Phys. Rev. D **99**, 012014 (2019).

[8] B. Aubert *et al.* (*BABAR* Collaboration), Phys. Rev. D **76**, 092005 (2007); **77**, 119902(E) (2008).

[9] J. P. Lees *et al.* (*BABAR* Collaboration), Phys. Rev. D **86**, 032013 (2012).

[10] J. P. Lees *et al.* (*BABAR* Collaboration), Phys. Rev. D **89**, 092002 (2014).

[11] J. P. Lees *et al.* (*BABAR* Collaboration), Phys. Rev. D **88**, 032013 (2013).

[12] A. Hoefer, J. Gluza, and F. Jegerlehner, Eur. Phys. J. C **24**, 51 (2002).

[13] K. I. Beloborodov, V. P. Druzhinin, and S. I. Serednyakov, J. Exp. Theor. Phys. **129**, 386 (2019).

[14] J. P. Lees *et al.* (*BABAR* Collaboration), Nucl. Instrum. Methods Phys. Res., Sect. A **726**, 203 (2013).

[15] B. Aubert *et al.* (*BABAR* Collaboration), Nucl. Instrum. Methods Phys. Res., Sect. A **479**, 1 (2002); B. Aubert *et al.* (*BABAR* Collaboration), Nucl. Instrum. Methods Phys. Res., Sect. A **729**, 615 (2013).

[16] J. P. Lees *et al.* (*BABAR* Collaboration), Phys. Rev. D **97**, 052007 (2018).

[17] N. N. Achasov and A. A. Kozhevnikov, Phys. Rev. D **55**, 2663 (1997).

[18] J. P. Lees *et al.* (*BABAR* Collaboration), Phys. Rev. D **98**, 112015 (2018).

[19] C. Bruch, A. Khodjamirian, and J. H. Kühn, Eur. Phys. J. C **39**, 41 (2005).